Table 1 Genotype of embryos from Syt heterozygous intercrosses

Embryonic day	Numbers of analyzed mice			
	+/+	+/−	−/− (abnormal[a])	Total
E7.5	8	4	5 (0)	17
E8.5	6	8	5 (0)	27
E9.5	202	411	190 (30)	803
E10.5	118	229	105 (51)	452
E11.5	25	60	21 (17)	106
E13.5	12	16	1 (1)	29
New born	90	112	0 (0)	202

[a]The number of embryos with a macroscopic abnormality is indicated in parentheses.

mately 50% of $Syt^{-/-}$ embryos were already dead as judged by heartbeats or the signs of re-absorption, and no $Syt^{-/-}$ homozygous mutants could be retrieved after E11.5 (Table 1). The $Syt^{-/-}$ embryos dissected at E9.75 were developmentally retarded in size (Figure 2a and b). The most severely affected but still viable mutant embryos usually displayed little or no signs of embryonic turning and exhibited only 10–14 somites (Figure 2c). We determined that the developmental arrest of $Syt^{-/-}$ embryos began at E8.5–E9.0, because generally, embryonic turning starts at E8.5 (8 somites) and is completed around E9.0 (16 somites).

Morphologically, all $Syt^{-/-}$ embryos could be distinguished from their wild-type littermates as early as E9.5 by their severe open neural tube as the neural tube begins to close at E8.5 and is completed by E9.0. These also suggest that developmental arrest of $Syt^{-/-}$ embryos was caused at E8.5–E9.0. In addition, various degrees of exencephaly were observed in $Syt^{-/-}$ embryos. Typically, the neural tube failed to fuse at the hindbrain and forebrain (Figure 2b and c). In the most severely affected mutants (data not shown), it remained completely open. Histological examination of E10.5 embryos revealed the exencephaly was caused by failure of neural tube closure (compare Figure 2d and e). The heterogeneity in the severity of Syt mutants indicates a partial penetration of the phenotypes possibly due to the genetic modifiers.

To identify the downregulated genes that are related to the phenotypes of $Syt^{-/-}$ mutants, we performed Gene Chip analysis using wild-type and $Syt^{-/-}$ embryos at E9.75. Many genes related to embryonic growth or neuronal development were downregulated in $Syt^{-/-}$ mutants (Supplementary Table 1).

As neural tube defects generally do not cause early embryonic lethality, we examined other developmental abnormalities in $Syt^{-/-}$ mutant embryos. While this study was in progress, another group reported the establishment of *Syt*-deficient mice,[17] exhibiting embryonic lethality between E8.5 and E9.5 either through an incomplete chorio-allantoic fusion or through a defect in the subsequent process of vascular branching morphogenesis.[17]

In contrast to the above-mentioned $Syt^{-/-}$ mice, almost all of our $Syt^{-/-}$ mutant embryos displayed normal chorio-allantoic fusion and exhibited normal labyrinth formation consisting of placental and embryonic vasculature at E9.75 (Figure 2f–k), even though their developmental stages were somewhat retarded. Thus, the embryonic lethality may not be due to the placental defect in our $Syt^{-/-}$ mutant embryos.

As placental defects did not provoke early embryonic lethality, at least before E9.5, we extensively examined other developmental abnormalities in our $Syt^{-/-}$ mutant embryos. At E9.5–E10.5, a number of $Syt^{-/-}$ mutants showed an enlarged cardiac cavity. Furthermore, $Syt^{-/-}$ mutants displayed severe pericardial effusions (Figure 2c), one of the clear signs of cardiac dysfunction. Cardiac ventricular movements appeared to be weaker and less expansive in mutants compared with that in wild-type embryos. Although no overt patterning defect was observed, the ventricular chambers of mutant embryos exhibited significantly thin wall and retarded maturation of trabeculation (Figures 2l–o, 4a and b).

Immunohistochemical Analysis of Syt-Deficient Mice

As the cardiac defect was found in $Syt^{-/-}$ embryos, we examined Gene Chip data of whole embryos focusing on cardiogenesis-specific genes. However, an obvious downregulation of cardiogenesis-specific genes was not observed in $Syt^{-/-}$ mutants (Supplementary Table 2).

Therefore, for better understanding the basis for the cardiac abnormality in the $Syt^{-/-}$ mutants, we analyzed whether cardiomyocytes undergo apoptosis by terminal deoxynucleotidyltransferase-mediated dUTP-biotin nick end labeling assay. In both wild-type and $Syt^{-/-}$ embryos, no significant induction of apoptosis was observed in various tissues (Figure 3a–d). Cell growth rates were also analyzed by immunostaining using antibodies for proliferation marker proteins, such as Ki-67 antigen and PCNA. The labeling indices of Ki-67 in the neural tube of wild-type embryos were higher than those in $Syt^{-/-}$ embryos at E10.5 (Figure 3e–h). In addition, immunostaining for PCNA showed that the growth rates of cardiomyocytes in $Syt^{-/-}$ embryos were much lower than those in wild-type embryos (Figure 3i–l). These results suggest that decreased cell growth may contribute to the impaired formation of cardiac ventricle in $Syt^{-/-}$ embryos.

Ultrastructural Analysis of the Heart in $Syt^{-/-}$ Embryos

For further analysis, we employed electron microscopy. First, we carefully prepared specimens from comparable areas of the ventricular free wall in both wild-type and $Syt^{-/-}$ embryos (Figure 4a and b). After, we confirmed the abnormality of the ventricular walls by toluidine blue staining, then the corresponding areas were subjected to electron microscopy. In cardiomyocytes of $Syt^{-/-}$ embryos at E10.5, the numbers

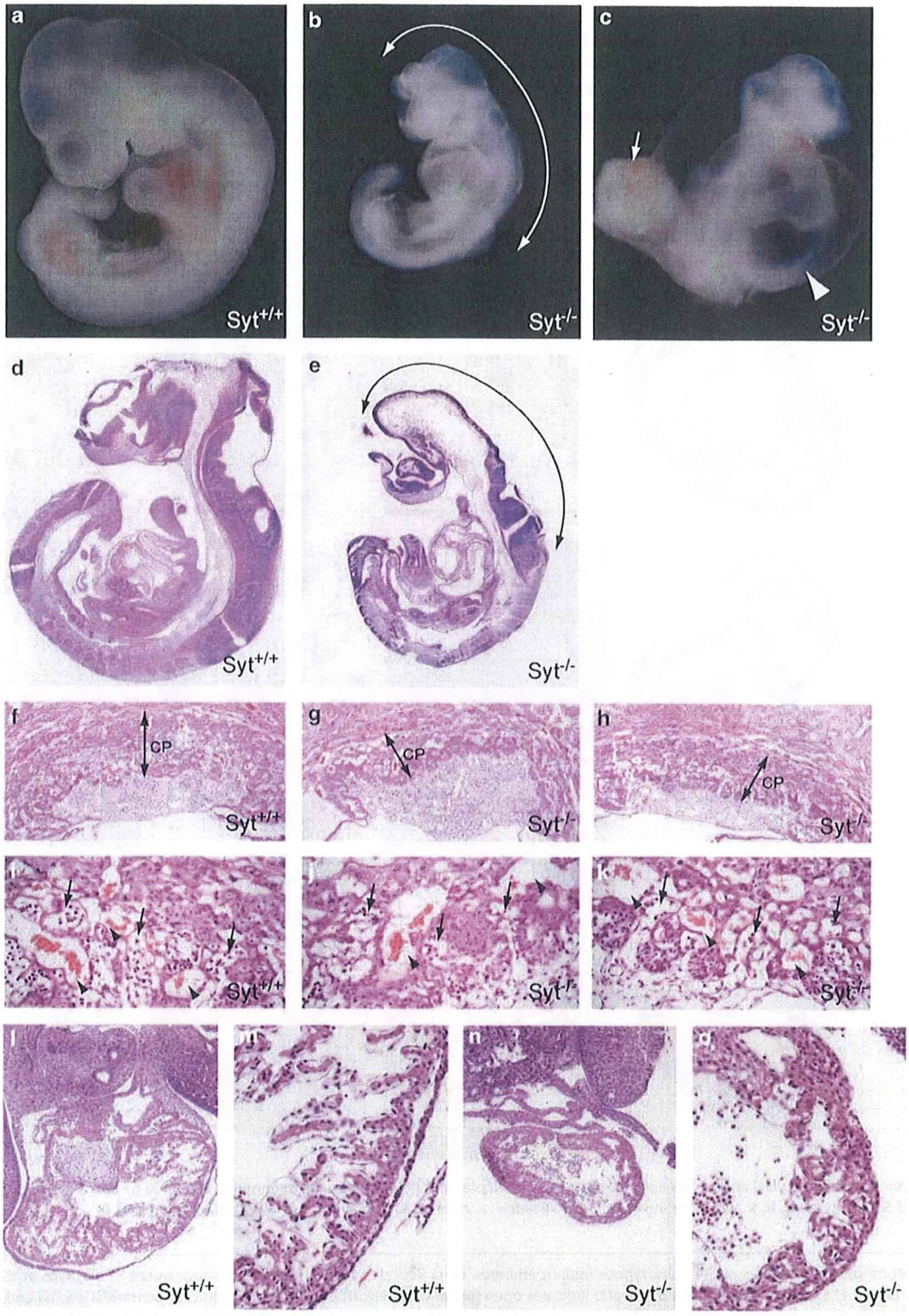
a
Syt+/+
b
Syt-/-
c
Syt-/-
d
Syt+/+
e
Syt-/-
f
CP
Syt+/+
g
CP
Syt-/-
h
CP
Syt-/-
i
Syt+/+
j
Syt-/-
k
Syt-/-
l
Syt+/+
m
Syt+/+
n
Syt-/-
o
Syt-/-

of perinuclear myofibrils and also of myofibrillar bundles were decreased (Figure 4c and d). Sarcomeric structure showed no significant difference between wild-type and $Syt^{-/-}$ mutant embryos (Figure 4e and f). Thus, cardiac development was perturbed in $Syt^{-/-}$ embryos, and this may be responsible for embryonic lethality.

Downregulation of p300 Expression in Syt-Deficient Mice

All $Syt^{-/-}$ homozygous mutants displayed lethality by E11.5, and among published gene knockout mice, especially those targeting chromatin modifiers, the phenotypes of $Syt^{-/-}$ mutants closely resembled those of p300-deficient mice.[18]

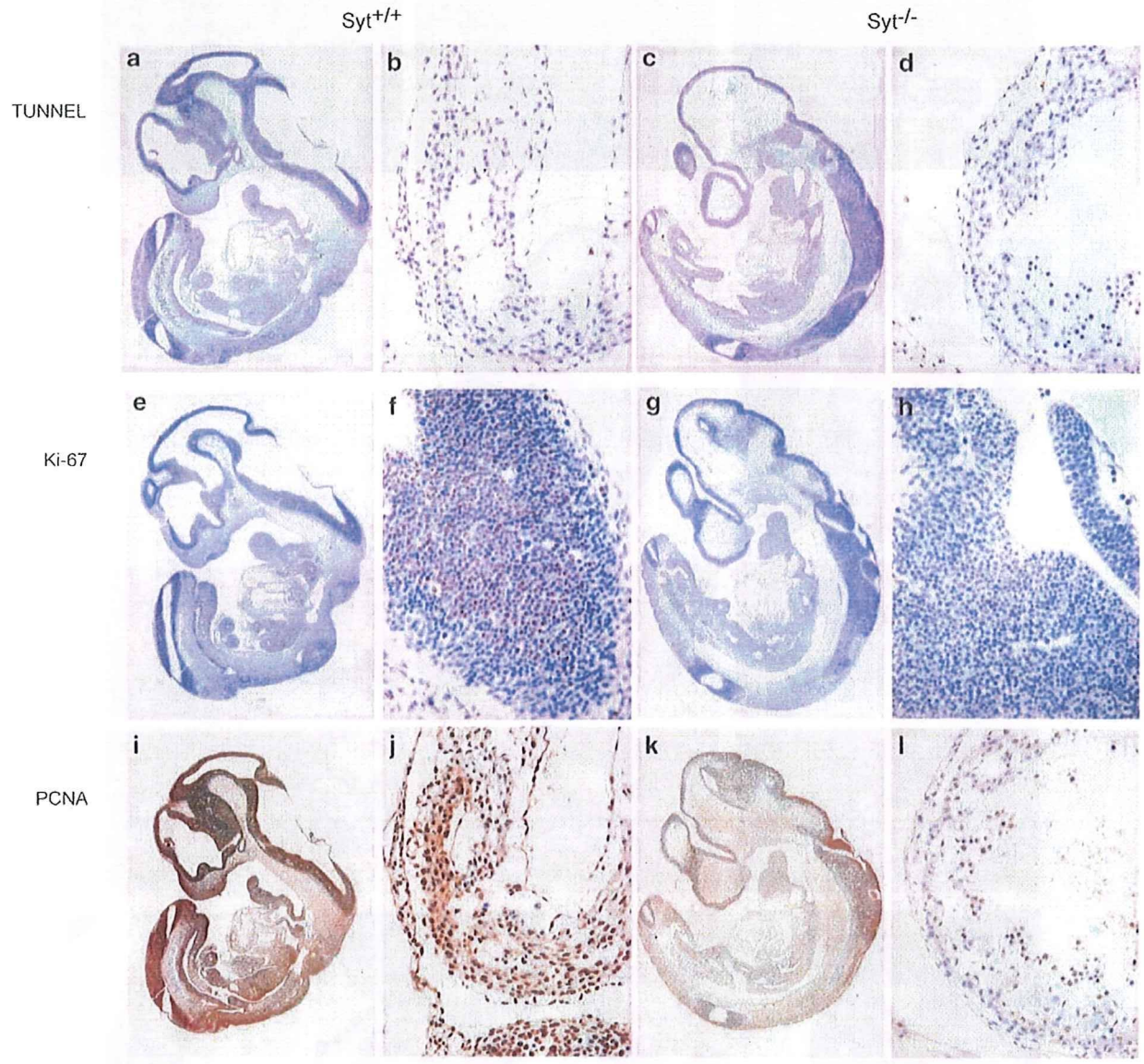

Figure 3 Immunohistochemical analysis for apoptosis and cell growth. (**a–d**) TUNEL staining; (**e–h**) immunostain for Ki-67 and (**i–l**) PCNA. $Syt^{+/+}$ (**a, b, e, f, i** and **j**) and $Syt^{+/-}$ (**c, d, g, h, k** and **l**) are indicated. Magnification × 20 (**a, c, e, g, i** and **k**) and × 400 (**b, d, f, h, j** and **l**).

Figure 2 Morphological analyses of Syt homozygous mutant embryos. (**a–c**) Representative stereoscopical appearance of embryos at E9.75 Syt+/+ (**a**) and $Syt^{-/-}$ (**b** and **c**). Double-headed arrow in panel b indicates open neural tube. Arrowheads in panel c indicate pericardial edema and arrow in panel c indicates allantois. (**d–o**) Microscopic analysis by H&E stain. Sagittal section of Syt+/+ (**d**) and $Syt^{-/-}$ (**e**) embryos at E10.5. Double-headed arrow in panel e indicates open neural tube. (**f–k**) Histopathology of $Syt^{+/+}$ (**f** and **i**) and $Syt^{-/-}$ (**g, h, j** and **k**) developing placenta at E9.75 (**i, j** and **k,** higher magnification of **f, g** and **h,** respectively). Double-headed arrows and CP in panels f–h indicate chorionic plate. Arrows in panels i–k indicate embryonic blood vessels, and arrowheads in panels i–k indicate maternal blood vessels, respectively. (**l–o**) Histopathology of Syt+/+ (**l** and **m**) and $Syt^{-/-}$ (**n** and **o**) embryonic heart at E10.5 (**m,** transverse section and **o,** higher magnification of **l** and **n,** respectively).

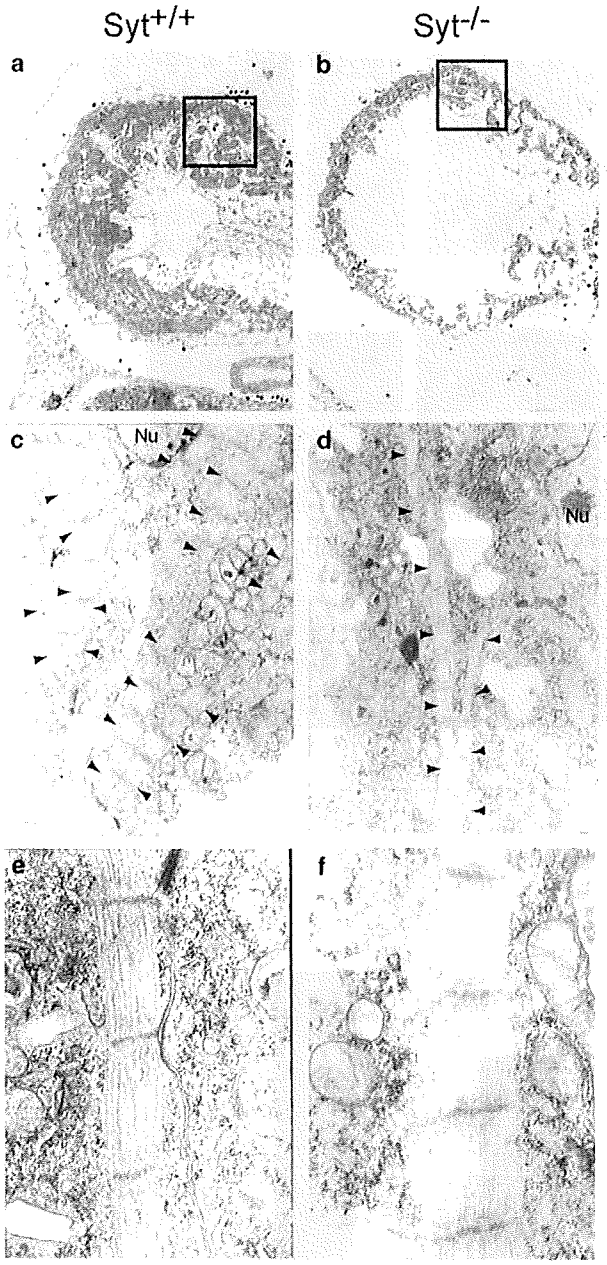

Figure 4 Ultrastructural analysis of embryonic hearts by transmission electron microscopy. (**a** and **b**) Toluidine blue stain for horizontal section of $Syt^{+/+}$ (**a**) and $Syt^{-/-}$ (**b**) embryos at E10.5. Squares indicate the areas subjected to EM analysis. (**c**–**f**) EM analysis of Syt+/+ (**a**, **c** and **e**) and $Syt^{-/-}$ (**b**, **d** and **f**) mutants with magnification × 5000 (**c** and **d**) and × 100 000 (**e** and **f**). Arrowheads in (**c**) and (**d**) indicate myofibrils. Nu, nuclei.

We, therefore, analyzed the expression levels of Syt-interacting proteins in $Syt^{-/-}$ embryos, focusing in particular on p300. We performed immunoblot analysis by using lysate of whole embryos of four individual lines of stage-matched $Syt^{+/+}$, $Syt^{+/-}$ and $Syt^{-/-}$ mutants, and found that the expression levels of p300 were significantly decreased in

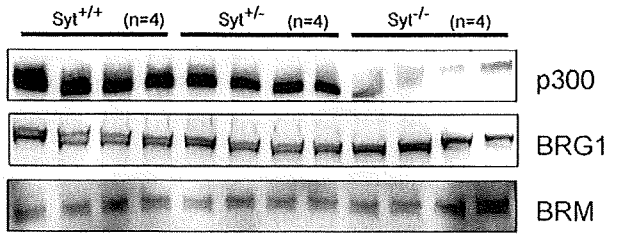

Figure 5 Immunoblot analysis of SYT-interacting proteins in Syt $^{-/-}$ embryos. Protein extracts (30 μg) from wild-type (lanes 1–4), heterozygous (lanes 5–8) and homozygous E10.5 embryos (lanes 9–12) were analyzed by immunoblotting using antibodies for p300, BRG1 and BRM.

$Syt^{-/-}$ homozygous mutants (Figure 5). In contrast, the expression levels of BRG1 and hBRM, which are components of SWI/SNF-type chromatin remodeling factors, were not significantly altered between the wild-type and Syt mutant embryos at E10.5 (Figure 5). These results suggest that Syt may regulate the expression level of p300, and the phenotype of the $Syt^{-/-}$ mutants may reflect at least in part the downregulation of p300.

Phenotypes of Syt-Deficient Mouse Embryonic Fibroblasts

To analyse the function of Syt in the cellular level, we established mouse embryonic fibroblasts from wild-type and $Syt^{-/-}$ embryos at E9.75. Interestingly, $Syt^{-/-}$ MEFs were morphologically different from wild-type MEFs (Figure 6a). Wild-type MEFs showed spindle shape, but in contrast, small rounded cells were dominant in $Syt^{-/-}$ MEFs (Figure 6a, left and right panels). In addition, in confluent culture, $Syt^{-/-}$ MEFs showed sheet cobble stone-like appearance (Figure 6a, center panel).

We next assessed whether Syt affects the formation of actin stress fibers and the localization of paxillin (a major constituent of focal adhesions) by confocal microscopy. Wild-type MEFs exhibited actin stress fiber formation and membrane ruffling; thus cell direction was readily recognized by leading edge (Figure 6b, upper left panel). In addition, localization of paxillin was diffusely observed in the cytoplasm dominantly seen at the ruffling side (Figure 6b, upper center panel).

In contrast, in small round cells, the dominant population in $Syt^{-/-}$ MEFs does not exhibit fine actin fibers but has a dense actin bundle below the plasma membrane (Figure 6b, lower center panel). Paxillin was localized only at the edge of the plasma membrane (Figure 6b, left panel), and we could not recognize directional morphology because of the loss of leading edge. For cell motility assessed by wound closure assay, after 17 h, wild-type MEFs covered most of the wounded area, but $Syt^{-/-}$ MEFs achieved only 35% (Figure 6c). Thus, Syt plays an important role in the motility of MEFs.

Expression of SYT-Interacting Proteins and Downregulated Gene Expression Profile in $Syt^{-/-}$ MEFs

To examine the molecular mechanisms of these phenotypes, we analyzed expression levels of Syt-interacting proteins in

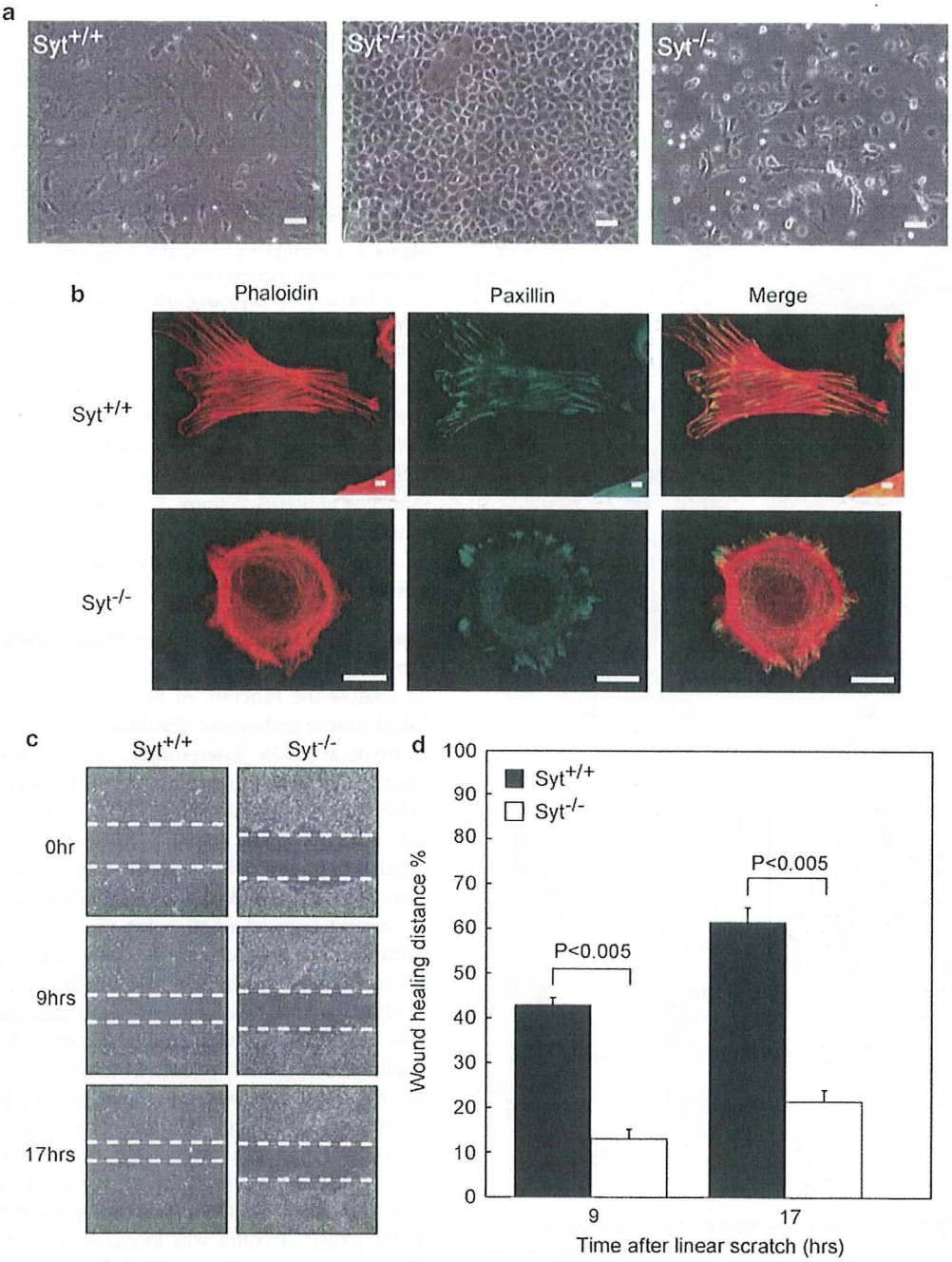

Figure 6 Phenotypical analysis of mouse embryonic fibroblasts established from $Syt^{-/-}$ embryos at E9.75. **(a)** Morphology of wild-type MEFs (right panel) and $Syt^{-/-}$ MEFs (center and left panels) in bright field. Scale bars, 50 μm. **(b)** Representative micrographs of immunocytofluorescence microscopy. Filamentous actin was visualized by phalloidin (right panels) and focal adhesions were visualized by anti-paxillin (center panels) in wild-type (upper panels) and $Syt^{-/-}$ (lower panels) MEFs, respectively. Scale bars, 10 μm. **(c)** Effect of Syt deficiency on motility inhibition. Representative micrographs at the indicated times after wounding. **(d)** Quantitative data from three independent experiments; columns, means, bars, s.d. (Student's *t*-test).

$Syt^{-/-}$ MEFs, especially focusing on participation of p300 in these phenotypes. We performed immunoblot analysis by using lysate from MEFs of the three individual lines (no. 237, no. 239 and no. 244) established from E9.75 embryos. Unexpectedly, unlike the result of the whole embryos, the expression level of p300 did not decrease in Syt $^{-/-}$ MEFs but showed various levels between wild-type and $Syt^{-/-}$ MEFs (Figure 7a). In addition, the expression levels of the other

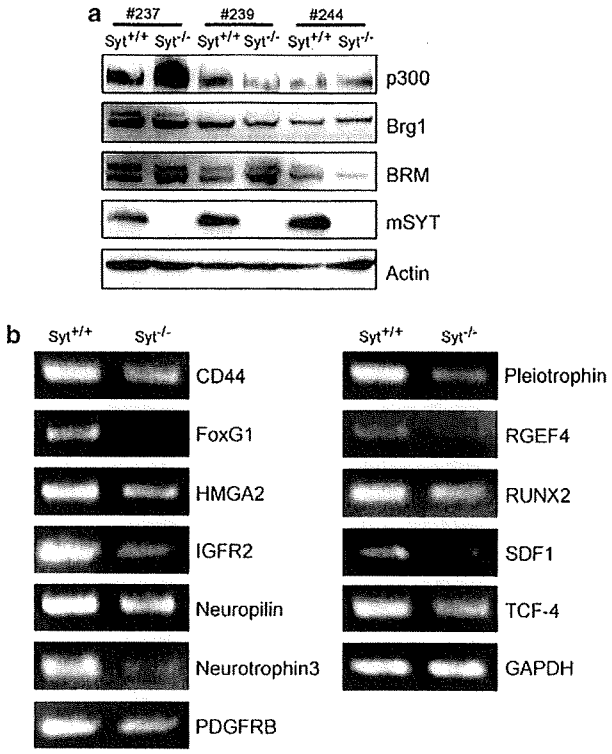

Figure 7 Expression of SYT-interacting proteins and downregulated gene expression in Syt $^{-/-}$ MEFs. **(a)** Immunoblot analysis of SYT-interacting proteins in Syt $^{-/-}$ MEFs. Three independent lines (no. 237, no. 239 and no. 244 indicate maternal mouse number) of MEFs established from E10.5 embryos of wild-type and Syt$^{-/-}$ were subjected to immunoblot analysis for p300, BRG1, hBRM, SYT and actin and are indicated at the right. Thirty micrograms of proteins were loaded in each lane. **(b)** Semi-quantitative RT-PCR analysis of gene expression downregulated in Syt$^{-/-}$ MEFs compared with wild type. Representative data of three independent experiments is shown.

Syt-interacting proteins were not significantly altered between wild-type and Syt$^{-/-}$ MEFs (Figure 7a). These data suggest that the expression level of p300 is not essential for the phenotypes of MEFs, at least, *in vitro*.

To identify the downregulated genes that are related to the phenotypes of Syt$^{-/-}$ MEFs, we performed Gene Chip analysis using wild-type and Syt$^{-/-}$ MEFs established from embryos at E9.75. Of a total of 22 691 genes analyzed, the expression of 2251 genes (5.41%) was significantly decreased by a factor of >3.0 in Syt$^{-/-}$ MEFs compared with wild-type MEFs (Table 2). Structural proteins, such as actin or myosin, matrix proteins, such as collagen, adhesion molecules, such as integrin or cadherin, cell surface receptors, such as CD44 or EphA7, and/or signal transducer, such as RGEF4, were downregulated in Syt$^{-/-}$ MEFs. To confirm these observations, we performed semi-quantitative RT-PCR expression analyses of these putative Syt target genes in other three independent sets of MEFs established from embryos at E9.75, and the microarray results for all 13 genes downregulated in all Syt$^{-/-}$ MEFs were tested (Figure 7b).

Table 2 Selected genes whose expression levels are downregulated in Syt$^{-/-}$ MEFs established from E9.75 embryos compared with wild-type as revealed by Gene Chip analysis

Accession no.	Gene product	Fold change[a]
Structural matrix		
NM_009610	Actin, γ-2, smooth muscle, enteric	−23.82
NM_013607	Myosin heavy polypeptide 11, smooth muscle	−20.66
NM_009925	Procollagen, type X, α-1	−15.77
NM_007733	Procollagen, type XIX, α-1	−13.96
M12233	Actin, α-1, skeletal muscle	−10.94
NM_007729	Procollagen, type XI, α-1	−9.18
AW412729	Procollagen, type XII, α-1	−6.74
AV246911	Procollagen, type V, α-1	−3.34
Transcription factor		
NM_008241	Forkhead box G1	−36.50
NM_010791	Mesenchyme homeobox 1	−22.62
NM_010441	High-mobility group AT-hook 2 (Hmga2)	−11.67
U16321	Transcription factor 4	−6.14
D14636	Runt-related transcription factor 2 (Runx2)	−3.23
Signal transduction		
NM_008742	Neurotrophin 3	−72.10
NM_008809	Platelet-derived growth factor receptor, β-polypeptide	−54.42
NM_015814	Dickkopf homolog 3 (Dkk3)	−29.39
BB623587	Integrin α-8	−27.47
AB021132	Rap guanine nucleotide exchange factor 4	−23.73
NM_008973	Pleiotrophin	−15.29
BB075797	Eph receptor A7	−12.68
NM_008737	Neuropilin	−6.41
BG066982	Natriuretic peptide receptor 3 (Npr3)	−4.93
NM_007631	Cyclin D1	−4.61
NM_130448	Protocadherin 18	−4.41
U04710	Insulin-like growth factor 2 receptor (Igf2r)	−4.01
BC005676	CD44	−3.80
U37029	Integrin β-1D	−3.71
NM_021704	Stromal cell-derived factor 1	−3.20
NM_011519	Syndecan 1	−3.00

[a]Genes are grouped according to the function of the encoded protein. '−' indicates the genes whose expression was downregulated in Syt$^{-/-}$ MEFs compared with that in wild-type MEFs.

DISCUSSION

To understand the biological role of Syt *in vivo*, we generated *Syt*-deficient mice and found that *Syt* deficiency exhibited embryonic lethality, open neural tube and cardiac dysfunction. $Syt^{-/-}$ mutant embryos showed that the defect of ventricular trabeculation and the phenotypes closely resemble those of p300-deficient mice. In fact, the expression levels of p300 were markedly decreased in Syt-deficient mice. Moreover, we isolated $Syt^{-/-}$ MEFs to elucidate the cellular basis of abnormalities in Syt-deficient embryos and showed that Syt participates in the regulation of actin fiber and cell motility.

While this work was in progress, another group reported the establishment of *Syt*-deficient mice, and they reported that Syt deficiency was lethal either through incomplete chorio-allantoic fusion or through a defect in the subsequent process of vascular branching morphogenesis.[17] Surprisingly, placental defect was rarely seen in our $Syt^{-/-}$ mutant embryos. The reason for this discrepancy is not clear, but may be due to differences in targeting strategies or in the genetic background of mice because of using different ES cells.

Syt was found to be essential for early embryogenesis and does not share functional redundancy with other proteins at least in the embryonic stage. In addition, $Syt^{+/-}$ heterozygous mutants showed haplo-insufficient lethality, which is a relatively rare phenotype in gene-disrupted mice. To our knowledge, haplo-insufficient lethality has been observed for p300, Dll4, Vezf1 and ROCK1.[19–21] During embryogenesis, the dosage of Syt may be critical for survival in a certain period *in utero* because newborn $Syt^{+/-}$ mutants lack overt defects. Once such $Syt^{+/-}$ embryos have completed gestation, the reduced Syt dosage does not seem to influence the growth of the newborns.

Normal placental development is initiated by the fusion of the chorionic and allantoic membranes (chorio-allantoic fusion) at E8.5 (8 somites),[22–24] thereby forming the chorionic plate, which is composed of trophoblasts. Through a subsequent process of vascular branching, fetal and maternal blood vessels enter this layer at E9.0, including the development of the placental labyrinth layer, which is made up of syncytiotrophoblasts, and at E10.0, the placenta becomes fully functional. The mutant mice in which the placenta is the only defective organ generally die no sooner than E9.5. In our mutant mice, the major defect begins before E8.5 at least, prior to the usual time of placental lethality. These data suggest that the main reason for our $Syt^{-/-}$ mutant's lethality was not likely to be the placental defect.

Although, morphologically, $Syt^{-/-}$ embryo displayed cardiac abnormalities, the expression levels of genes being essential for cardiac development, including GATA4, MEF2C, Nkx2.5 and so on,[25] were not decreased in $Syt^{-/-}$ embryos. As the proportion of cardiogenesis-specific transcription factor transcripts is very small compared with total embryo mRNA, the difference between wild-type and mutant embryos may not be detectable by this approach.

Interestingly, these embryonic neural and cardiac phenotypes of $Syt^{-/-}$ embryos closely resemble those of p300-deficient mice.[18] On the basis of our data showing that protein levels of p300 were decreased in $Syt^{-/-}$ embryos, Syt may regulate cardiac ventricular maturation through the control of p300 expression.

It was also reported that the SWI/SNF type of chromatin remodeling complex, such as BAF60c and BAF180, has been shown to be required for cardiogenesis.[26,27] In fact, we have found that Syt binds to the complete BAF complex by MALDI-TOF mass spectrometry (T Kimura, unpublished data). Thus, in the absence of Syt, the deregulation of BRG1 together with p300 possibly underlies the defects in the proteins closely related to myofibril formation.

Syt-deficient cells with actin fiber deregulation and suppressed motility might explain the developmental problem. One possible mechanism is that complex formation of SYT and p300, and not only the amount of p300, may regulate cell motility. It was reported that SYT/p300 complex promotes cell adhesion by regulating β1 integrin/fibronectin receptor function.[11] In fact, our Gene Chip analysis showed that integrin β1D and integrin α8, which form heterodimeric transmembrane receptor for fibronectin,[28] were downregulated in $Syt^{-/-}$ MEFs. Thus, p300/SYT complex possibly regulates cell motility through the β1 integrin and/or α8 integrin.

Alternatively, Syt regulated cell migration through the transcriptional regulation of Rap guanine nucleotide exchange factor 4 (now designated as Epac2), which is one of the decreased genes in $Syt^{-/-}$ MEFs. Epac2 was initially characterized as a cAMP-activated GEF for Rap1 and Rap2,[29,30] and as a novel sensor for several pivotal cellular processes, including cell polarization, integrin-mediated cell adhesion, cell migration and cytoskeletal rearrangements through the regulation of Rap, Rho, Ras and Rac.[31–34] As such, we think the possibility that Syt regulates Ras and Rho superfamily through the transcriptional regulation of Epac2.

In this study, we discovered new phenotypes of Syt, such as poor ventricular trabeculation and downregulation of p300 protein in $Syt^{-/-}$ whole embryos. In addition, by the establishment of $Syt^{-/-}$ MEFs, we uncovered that Syt plays an important role in the regulation of cell motility. Thus, $Syt^{-/-}$ MEFs must be one of the useful materials to analyze Syt functions in detail. In future, we will study the association between Syt and malignant human cancer such as synovial sarcoma.

Supplementary Information accompanies the paper on the Laboratory Investigation website (http://www.laboratoryinvestigation.org)

ACKNOWLEDGEMENTS

We thank Dr Ken Sasai (Hokkaido University) and Hiroaki Hiraga (Sapporo Cancer Center) for useful suggestions. This study was supported in part by grants-in-aid from the Ministry of Education, Science, Culture, and Sports, and from the Ministry of Health, Labor, and Welfare; and also by the

YASUDA Medical Research Foundation, by the Suhara Foundation, by the Mochida Memorial Foundation for Medical and Pharmaceutical Research and by the UEHARA Medical Research Foundation.

1. Ladanyi M. Fusions of the SYT and SSX genes in synovial sarcoma. Oncogene 2001;20:5755–5762.
2. Lewis JJ, Antonescu CR, Leung DH, *et al.* Synovial sarcoma: a multivariate analysis of prognostic factors in 112 patients with primary localized tumors of the extremity. J Clin Oncol 2000;18:2087–2094.
3. Clark J, Rocques PJ, Crew AJ; *et al.* Identification of novel genes, SYT and SSX, involved in the t(X;18)(p11.2;q11.2) translocation found in human synovial sarcoma. Nat Genet 1994;7:502–508.
4. dos Santos NR, de Bruijn DR, van Kessel AG. Molecular mechanisms underlying human synovial sarcoma development. Genes Chromosomes Cancer 2001;30:1–14.
5. Thaete C, Brett D, Monaghan P, *et al.* Functional domains of the SYT and SYT–SSX synovial sarcoma translocation proteins and co-localization with the SNF protein BRM in the nucleus. Hum Mol Genet 1999;8:585–591.
6. Brett D, Whitehouse S, Antonson P, *et al.* The SYT protein involved in the t(X;18) synovial sarcoma translocation is a transcriptional activator localized in nuclear bodies. Hum Mol Genet 1997;6:1559–1564.
7. Nagai M, Tanaka S, Tsuda M, *et al.* Analysis of transforming activity of human synovial sarcoma-associated chimeric protein SYT–SSX1 bound to chromatin remodeling factor hBRM/hSNF2 alpha. Proc Natl Acad Sci USA 2001;98:3843–3848.
8. Kato H, Tjernberg A, Zhang W, *et al.* SYT associates with human SNF/SWI complexes and the C-terminal region of its fusion partner SSX1 targets histones. J Biol Chem 2002;277:5498–5505.
9. Ishida M, Tanaka S, Ohki M, *et al.* Transcriptional co-activator activity of SYT is negatively regulated by BRM and Brg1. Genes Cells 2004;9:419–428.
10. de Bruijn DR, dos Santos NR, Thijssen J, *et al.* The synovial sarcoma associated protein SYT interacts with the acute leukemia associated protein AF10. Oncogene 2001;20:3281–3289.
11. Eid JE, Kung AL, Scully R, *et al.* p300 interacts with the nuclear proto-oncoprotein SYT as part of the active control of cell adhesion. Cell 2000;102:839–848.
12. Ito T, Ouchida M, Ito S, *et al.* SYT, a partner of SYT–SSX oncoprotein in synovial sarcomas, interacts with mSin3A, a component of histone deacetylase complex. Lab Invest 2004;84:1484–1490.
13. Nakayama K, Ishida N, Shirane M, *et al.* Mice lacking p27(Kip1) display increased body size, multiple organ hyperplasia, retinal dysplasia, and pituitary tumors. Cell 1996;85:707–720.
14. Sambrook J, Maniatis T, Fritsch EF. Molecular Cloning. A Laboratory Manual, 2nd edn. Cold Spring Harbor Laboratory: NY, 1989.
15. Yang JT, Rayburn H, Hynes RO. Embryonic mesodermal defects in α5 integrin-deficient mice. Development 1993;119:1093–1105.
16. Defilippi P, Truffa G, Stefanuto G, *et al.* Tumor necrosis factor a and interferon g modulate the expression of the vitronectin receptor (integrin h3) in human endothelial cells. J Biol Chem 1991;266:7638–7645.
17. de Bruijn DR, Peters WJ, Chuva de Sousa Lopes SM, *et al.* Targeted disruption of the synovial sarcoma-associated SS18 gene causes early embryonic lethality and affects PPARBP expression. Hum Mol Genet 2006;15:2936–2944.
18. Yao TP, Oh SP, Fuchs M, *et al.* Gene dosage-dependent embryonic development and proliferation defects in mice lacking the transcriptional integrator p300. Cell 1998;93:361–372.
19. Gale NW, Dominguez MG, Noguera I, *et al.* Haploinsufficiency of delta-like 4 ligand results in embryonic lethality due to major defects in arterial and vascular development. Proc Natl Acad Sci USA 2004;101:15949–15954.
20. Kuhnert F, Campagnolo L, Xiong JW, *et al.* Dosage-dependent requirement for mouse Vezf1 in vascular system development. Dev Biol 2005;283:140–156.
21. Zhang YM, Bo J, Taffet GE, *et al.* Targeted deletion of ROCK1 protects the heart against pressure overload by inhibiting reactive fibrosis. FASEB J 2006;20:916–925.
22. Cross JC. Genetic insights into trophoblast differentiation and placental morphogenesis. Semin Cell Dev Biol 2000;11:105–113.
23. Rossant J, Cross JC. Placental development: lessons from mouse mutants. Nat Rev Genet 2001;2:538–548.
24. Hemberger M, Cross JC. Genes governing placental development. Trends Endocrinol Metab 2001;12:162–168.
25. Srivastava D, Olson EN. A genetic blueprint for cardiac development. Nature 2000;407:221–226.
26. Lickert H, Takeuchi JK, Von Both I, *et al.* Baf60c is essential for function of BAF chromatin remodelling complexes in heart development. Nature 2004;432:107–112.
27. Wang Z, Zhai W, Richardson JA, *et al.* Polybromo protein BAF180 functions in mammalian cardiac chamber maturation. Genes Dev 2004;18:3106–3116.
28. Brakebusch C, Fassler R. β1 integrin function *in vivo*: adhesion, migration and more. Cancer Metastasis Rev 2005;23:403–411.
29. de Rooij J, Zwartkruis FJ, Verheijen MH, *et al.* Epac is a Rap1 guanine nucleotide-exchange factor directly activated by cyclic AMP. Nature 1998;396:474–477.
30. Kawasaki H, Springett GM, Mochizuki N, *et al.* A family of cAMP-binding proteins that directly activate Rap1. Science 1998;282:2275–2279.
31. Bos JL. Linking Rap to cell adhesion. Curr Opin Cell Bio 2005;17:123–128.
32. Gupta M, Yarwood SJ. MAP1A light chain 2 interacts with exchange protein activated by cyclic AMP 1 (EPAC1) to enhance Rap1 GTPase activity and cell adhesion. J Biol Chem 2005;280:8109–8116.
33. Del Pozo MA, Alderson NB, Kiosses WB, *et al.* Integrins regulate Rac targeting by internalization of membrane domains. Science 2004;303:839–842.
34. Rangarajan S, Enserink JM, Kuiperij HB, *et al.* Cyclic AMP induces integrin-mediated cell adhesion through Epac and Rap1 upon stimulation of the beta 2-adrenergic receptor. J Cell Biol 2003;160:487–493.